Thermal Emission Spectra from Individual Suspended Carbon Nanotubes

Zuwei Liu,[†] Adam Bushmaker,[‡] Mehmet Aykol,[‡] and Stephen B. Cronin[†,‡,*]

[†]Department of Physics and [‡]Department of Electrical Engineering, University of Southern California, Los Angeles, California 90089, United States

ABSTRACT We study the thermal emission spectra of individual suspended carbon nanotubes induced by electrical heating. Semiconducting and metallic devices exhibit different spectra, based on their distinctive band structures. These spectra are compared with the ideal blackbody emission spectrum. In the visible wavelength range, the thermal emission spectra of semiconducting devices agree well with Planck's law, while the spectra of metallic devices show an additional peak between 1.5 and 1.9 eV. In the near-infrared wavelength range, the semiconducting nanotubes exhibit a peak around 1 eV. These additional peaks are attributed to the E_{11}^{M} and E_{22}^{SC} transitions that are thermally driven under these high applied bias voltages. These peaks show a strong polarization dependence, while the blackbody tail is unpolarized, which provides further evidence for electron−hole recombination in thermal emission. For semiconducting devices, the temperature of the nanotube is fit to Planck's law and compared with the temperatures obtained from the G band and 2D band Raman downshifts, as well as the anti-Stokes/Stokes intensity ratio. For devices showing thermal non-equilibrium, the electron temperature agrees well with G_+ downshift but deviates from G_- downshift.

KEYWORDS: carbon nanotube · thermal emission · photon · Raman spectrum · phonon · transition

Since their discovery 20 years ago, the electrical properties of carbon nanotubes have included reports of coulomb blockade,[1] ballistic electron conduction,[2] negative differential resistance,[3] Mott insulating states,[4] and Luttinger liquid behavior.[5] The mechanism by which electrons dissipate heat to the lattice is particularly interesting in this remarkable one-dimensional system. The current-carrying capacity of nanotubes exceeds that of the noble metals (*e.g.*, Au and Ag) by several orders of magnitude.[6] Because of their one-dimensional nature, acoustic phonon scattering is strongly suppressed in carbon nanotubes (CNTs). As a result, optical phonon scattering is the dominant mechanism in carbon nanotubes. This scattering mechanism was first proposed to explain current saturation in metallic nanotubes at high bias voltages.[7] This results in ballistic electron transport at low bias voltages and optical phonon scattering at high bias voltages. Pop *et al.* further demonstrated this mechanism in suspended, nearly defect-free carbon nanotubes, which exhibited negative differential resistance (NDR) as a result of this threshold optical phonon emission process.[3] Several theoretical works have investigated the high bias transport in CNTs.[8,9]

The phonon temperatures of electrically heated carbon nanotube devices have been studied extensively by our group[10−12] and others.[13,14] For electrically heated graphene, the thermal emission spectra can be fit easily using Planck's law, and these temperatures have been found in close agreement with phonon temperatures measured by Raman spectroscopy.[15,16] Electrically driven thermal emission from multiwall carbon nanotube bundles has also shown featureless blackbody emission that can be easily interpreted using Planck's law.[17,18] For MWNTs, the density of states is quite uniform, thus behaving like a free electron gas in a bulk metal. More recently, studies have concentrated on individual single-wall carbon nanotubes with sharp van Hove singularities, including measurements of both on-substrate[19,20] and suspended metallic carbon nanotubes.[20−24] However, an accurate extraction of the temperature is lacking in these works because the emission spectra deviate significantly from Planck's law due to their complicated band structure. Wang *et al.* have attempted to extract the temperature from the blackbody tail using a reduced Planck law (*i.e.*, $\exp(-E/K_BT)$). However, this is not accurate and tends to overestimate the temperature, as discussed below. Additional peaks in the thermal emission spectra of metallic carbon nanotubes have been reported by several groups.[19−21] Various possible mechanisms have been put forth to explain the thermal emission peaks observed in these nanotubes, including electronic transitions between van Hove

* Address correspondence to scronin@usc.edu.

Received for review February 2, 2011 and accepted May 5, 2011.

Published online May 05, 2011
10.1021/nn200444x

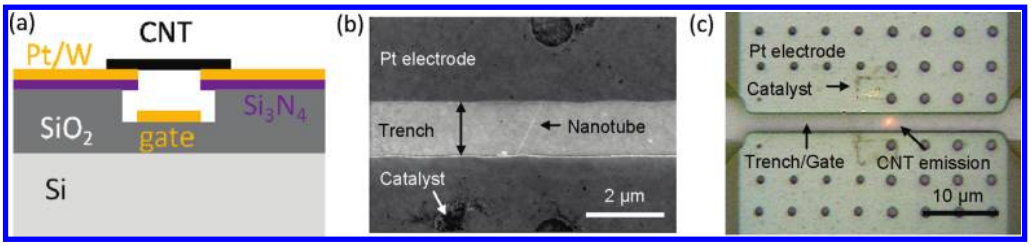

Figure 1. (a) Diagram of device cross section. (b) SEM image and (c) optical microscope image of device showing thermal emission.

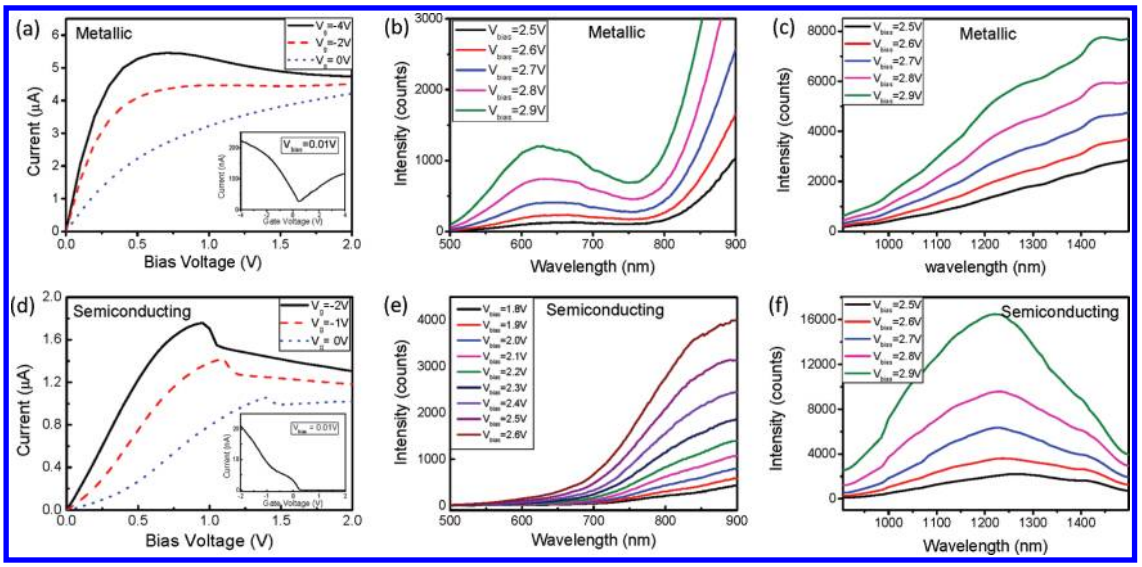

Figure 2. *I*−*V* characteristics and corresponding thermal emission spectra taken at a gate voltage of −2 V of (a−c) a metallic and (d−f) a semiconducting device, respectively.

singularities,[21] phonon-assisted interband transitions,[20] and phonon-assisted decay from the π^* band state at the M point to the Fermi level at K point in the Brillouin zone.[19] Further investigation is needed to establish/verify the mechanism underlying these peaks.

In our work, the thermal emission spectra of both metallic and semiconducting suspended carbon nanotubes are compared to ideal blackbody emission. The advantage of suspended devices is that the interaction between the device and its underlying substrate can be ignored, and thus the emission spectrum is entirely from the individual nanotubes under investigation. These suspended nanotubes also exhibit non-equilibrium phonon populations,[10] making this thermal emission temperature measurement especially important. By comparing both metallic and semiconducting CNT devices, we can rule out several possible mechanisms that have been previously proposed. The polarization dependence of the various features in the emission spectra provides further information about these peaks. Lastly, by comparing the temperature extracted from the thermal emission spectra with those obtained from Raman spectroscopy, we are able to provide a reliable method for interpreting the temperature from these thermal emission spectra observed under high bias voltages.

RESULTS AND DISCUSSION

Figure 2 shows the *I*−*V* curves and thermal emission spectra of a metallic (Figure 2a−c) and a semiconducting (Figure 2d−f) device. Both devices show negative differential conductance (NDC) in the high bias regime, due to optical phonon scattering.[3,7,10,26] The elevated temperatures reached in the NDC region enable clear observation of the devices' thermal emission spectra. Among the 11 devices measured in this study, the emission spectra of all semiconducting nanotubes in the wavelength range between 500 and 900 nm resemble blackbody emission from Planck's law, while all metallic nanotubes show an additional peak between 635 and 783 nm.

Panels c and f of Figure 2 show the near-infrared spectra of a metallic and a semiconducting device measured with an InGaAs detector from 900 to 1500 nm. In this wavelength range, the metallic nanotube shows blackbody emission, while the semiconducting nanotube shows a peak around 1215 nm. These additional peaks (635 nm for metallic and 1215 nm for semiconducting nanotubes) correspond

TABLE 1. Summary of Peak Emission Energies Observed in Five Semiconducting and Six Metallic Nanotubes at V_{bias} = 2.0 V for Metallic Nanotubes and V_{bias} = 2.5 V for Semiconducting Nanotubes

semiconducting peaks (nm):	1114, 1117, 1157, 1158, 1215
metallic peaks (nm):	635, 742, 748, 769, 776, 783

to the E_{11}^{M} transitions in metallic and E_{22}^{SC} transitions in semiconducting nanotubes. Under high bias voltages, the thermal population of these sub-bands becomes significant, leading to electron−hole relaxation and the emission of photons.

Table 1 lists the peak emission energies observed in five semiconducting and six metallic nanotubes, which range from 1114 to 1215 nm and from 635 to 783 nm, respectively. Here, the emission peak energies are given for the metallic nanotube spectra taken at V_{bias} = 2.0 V and the semiconducting spectra at V_{bias} = 2.5 V. The peaks were fit after normalizing to the spectral response of the system, as calibrated by a blackbody tungsten source. This procedure is described in the Supporting Information. Figure 3 shows the optical transition energies of SWNTs plotted as a function of nanotube diameter, taken from Araujo *et al.*[27] Unfortunately, no photoluminescence or radial breathing modes were observed for these nanotubes. However, using the same growth conditions, we have observed RBMs from a total of 55 devices. A histogram of the corresponding diameters is plotted in Figure 3b, which shows a distribution centered around 1.45 ± 0.15 nm. For semiconducting nanotubes in this diameter range, the band gap E_{11}^{SC} lies below the minimum cutoff energy of the InGaAs detector. As a result, we were not able to observe any band gap or sub-band gap emission. The deviation of the thermal emission spectra of carbon nanotubes from pure blackbody emission spectra is due electron−hole recombination at E_{11}^{M} and E_{22}^{SC} in the carbon nanotubes.[28] However, these peaks in the thermal emission spectra are considerably broader than the corresponding peaks in absorption and photoluminescence spectra of individual CNTs[29] because of the recombination of thermally excited electron−hole pairs with energies greater than E_g, as discussed below.

Figure 4 shows the polarization dependence of the thermal emission spectra of a metallic carbon nanotube. The peak observed around 740 nm due to electron−hole recombination exhibits a strong polarization dependence, while the blackbody tail extending into the near-infrared does not. We observe a similar behavior for semiconducting nanotubes, where the peaks around 1150 nm are strongly polarized. Li *et al.*[18] suggested that polarized incandescent light is emitted from MWNTs because the electrons can only be accelerated and decelerated along the nanotube axis.[18] In this case, the whole spectrum should be polarized in the same way. However, our results show that the polarization only occurs at specific energies

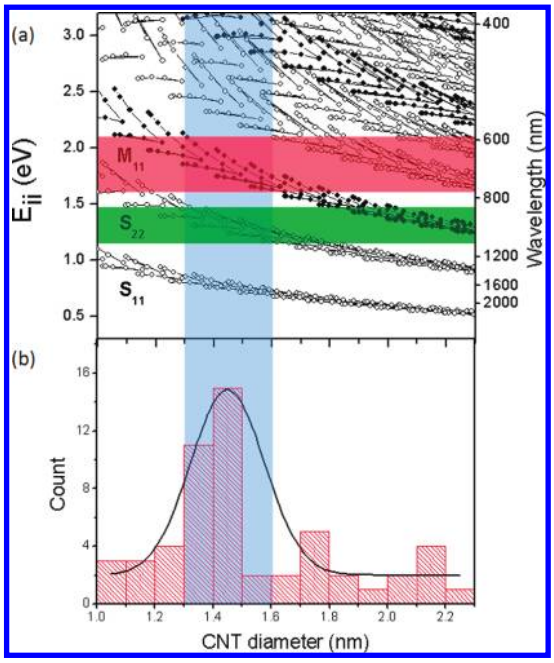

Figure 3. (a) Kataura plot of the electronic transition energies of carbon nanotubes. (b) Histogram of CNT diameter distribution based on RBM measurements from 55 single nanotube devices.

corresponding to electronic transitions, while the blackbody tail is independent of polarization angle. The corresponding NIR data for this device are shown in Figure S4 of the Supporting Information, which shows no polarization dependence.

The temperatures of these suspended CNT devices obtained by fitting the thermal emission spectra to Planck's law were compared with those obtained from Raman spectroscopy. We fit our thermal emission spectra using Planck's equation

$$I(\lambda) = \frac{C_1}{\lambda^5} \frac{1}{\exp\left(\frac{hc}{\lambda k_B T}\right) - 1} \quad (1)$$

where C_1 is a constant and T is the fitting parameter. We use a tungsten lamp covered by a 5 μm pinhole as a calibration source. The actual temperature of the tungsten lamp can be determined from its change in resistance.[30] On the basis of this calibration from 500 to 800 nm, the temperature fit by eq 1 agrees very well with its actual temperature. The error is within 50 K from 900 to 1600 K. However, if we use the reduced Planck law (*i.e.*, $\exp(-E/K_BT)$), the fitted temperature is higher than the real temperature by more than 200 K. A discussion of the error in this measurement is given the Supporting Information.

Temperatures are also obtained from the calibrated downshifts of the G band Raman frequency.[31] For the device shown in Figure 2d, the G_+ downshift (Figure 5b) agrees very well with that of the anti-Stokes G band downshift; however, the slope of the G_- downshift is smaller, indicating the non-equilibrium coupling of

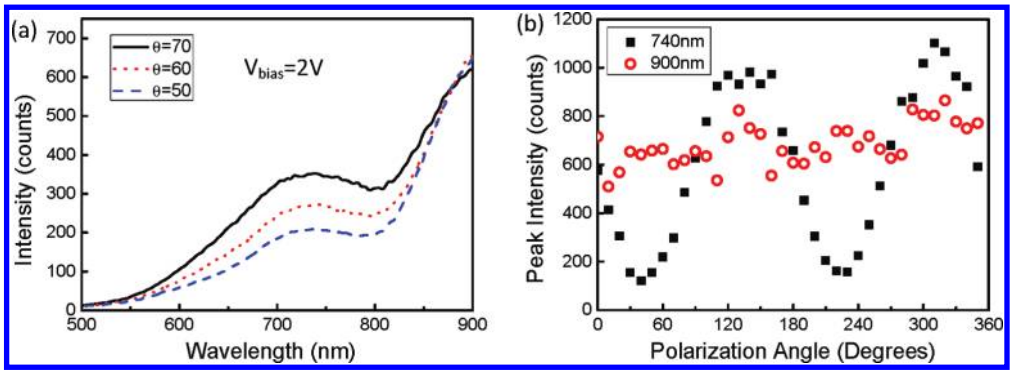

Figure 4. Polarization dependence of thermal emission spectra of a metallic CNT.

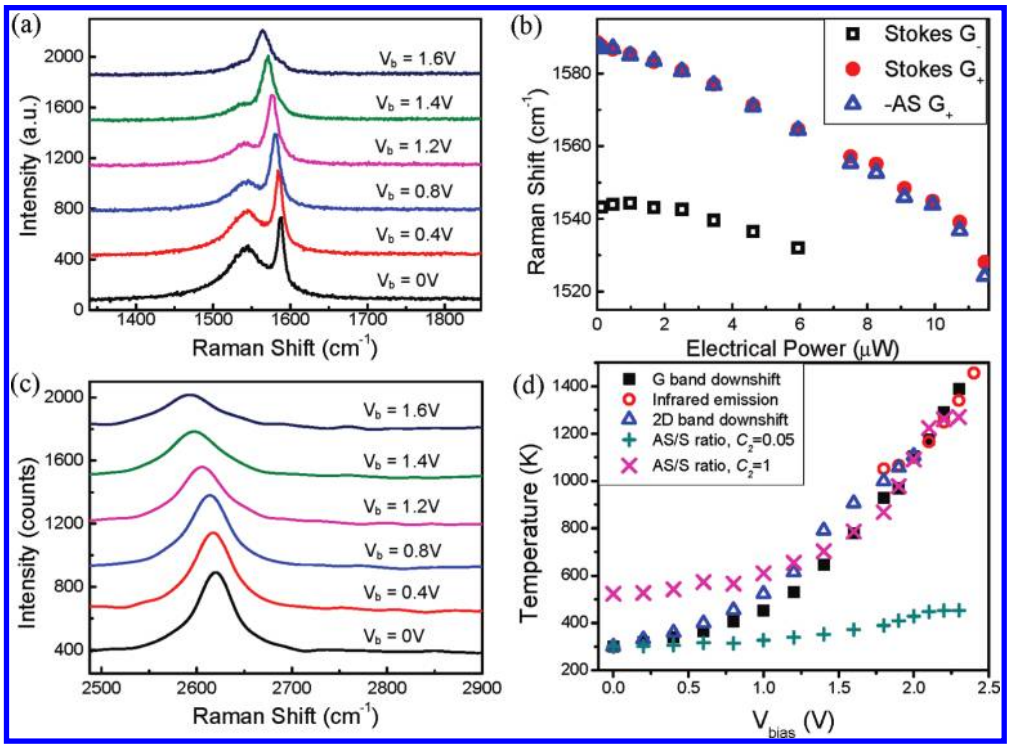

Figure 5. (a,b) G band and (c) 2D band downshift of a semiconducting CNT device under various applied bias voltages. (d) Bias voltage dependence of CNT temperature as determined from G band downshift, Stokes/anti-Stokes ratio, 2D band downshift, and thermal emission spectra in the NDC regime.

electrons with TO and LO phonons, as reported previously.[10] Figure 5c shows the Raman shift of the 2D band under applied bias voltages for the same device. In addition to the downshift of the 2D band, we also observe broadening of the 2D band, as the temperature increases. Once the 2D band downshift slope is also calibrated using a temperature-controlled stage, the device temperature can be calculated, assuming a linear relation between the temperature and Raman downshift.

The anti-Stokes/Stokes (AS/S) Raman intensity ratio is given by the equation

$$\frac{I_{aS}}{I_S} = C_2 \frac{E_L^3}{(E_L - \hbar\omega_{ph})^3} \exp\left(-\frac{\hbar\omega_{ph}}{k_B T_{op}}\right) \qquad (2)$$

Here, the constant C_2 is included to account for the resonance condition, which was calibrated at room temperature to be equal to 0.05. However, it is likely that C_2 changes significantly with temperature because the resonant optical transition energies change with temperature.[32] This results in the large deviation from the other temperatures in Figure 5d. In this plot, we used the calibrated value of $C_2 = 0.05$ to estimate the lower limit of device temperature and $C_2 = 1$ for calculating the upper limit. While this represents a large range of uncertainty, these data sets agree quite well with the other temperatures in the two extremes of low and high temperature.

Figure 5d shows a comparison of the CNT temperatures obtained from the G band downshift, infrared

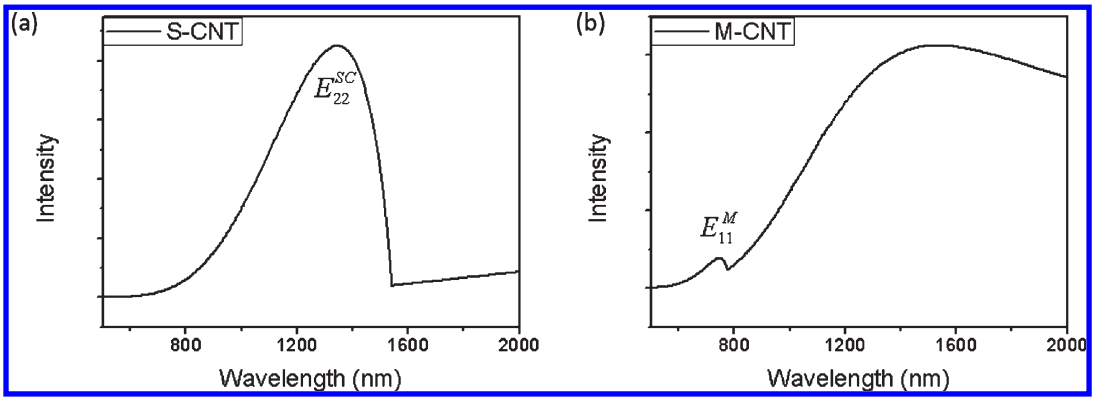

Figure 6. Calculated thermal emission spectra for (a) a semiconducting nanotube and (b) a metallic nanotube.

emission, and the AS/S Raman intensity ratio. Here, we observe good agreement in the intermediate range of bias voltages. At low bias, the IR emission is not accurate because of the low signal-to-noise ratio. At high bias, the AS/S ratio does not give an accurate temperature, as the nanotube shifts off of resonance with the incident laser, as discussed above. In the intermediate range, however, good agreement can be seen between the various temperatures. It should be noted, however, that for the nanotube diameter distribution in this work (1.45 ± 0.15 nm), the higher energy transitions E_{33} and E_{44} (2.5 and 3.5 eV) lie beyond the range of our detector (2.4 eV), enabling us to fit the blackbody tail of these spectra and extract meaningful temperature data. For a different range of diameters, it may be necessary to adjust this energy window in order to extract the temperature reliably.

In order to understand the origin of the peaks in the thermal emission spectra of semiconducting and metallic nanotubes, we use a simple model based on their electronic density of states. Here, we assume that thermally excited hot electrons transition from a high energy state to a low energy state with a probability proportional to the electron population at the high energy state and the hole population at the low energy state. While the optical transitions in carbon nanotubes are excitonic in nature, we use a simple band-to-band model here to explain our experimental results. The exciton binding energies in semiconducting and metallic nanotubes are on the order of 1 eV and 100 meV, respectively, which significantly downshift the electronic transition energies from the single particle band-to-band energies.[33] However, the self-energy (band gap renormalization) in nanotubes is also quite large and results in an upshift, which places the actual electronic transition energies close to the single particle band-to-band energies.[34,35] While a full treatment including the effects of excitons is beyond the scope of this paper, this model demonstrates that the thermal populations of E_{11}^{M} and E_{22}^{SC} are large enough to produce a significant contribution to the thermal radiation, which results in a deviation from blackbody emission. From an energy conservation point of view, the down-transition, which emits photons, and the up-transition, which takes electrical power, are in equilibrium. At temperature T, the population of electrons and holes can be calculated from the Fermi distribution and the density of states as follows.

$$P_e(E + E_{ph}) \propto f(E + E_{ph})\mathrm{DOS}(E + E_{ph}) \quad (3)$$

and

$$P_h(E) \propto (1 - f(E))\mathrm{DOS}(E) \quad (4)$$

where P_e and P_h are the populations of electrons and holes, E_{ph} is the energy of the emitted photon, f is the Fermi distribution, and DOS represents the density of states. We then represent the total photon power radiated as

$$R(E_{ph}) \propto \int_E P_e(E + E_{ph})E_{ph}P_h(E)dE \quad (5)$$

Figure 6a,b shows the calculated emission spectra of a semiconducting nanotube with E_{22}^{SC} = 0.8 eV and a metallic nanotube with E_{11}^{M} = 1.6 eV. From the calculation, we can see that the thermal emission spectra include both intraband transitions, which contribute to the blackbody background, and electronic transitions at E_{11}^{M} and E_{22}^{SC}.

CONCLUSION

In conclusion, we compare the thermal emission spectra of metallic and semiconducting suspended carbon nanotubes under high bias voltages. The spectra indicate that electron−hole recombination at the E_{11}^{M} and E_{22}^{SC} transitions plays an important role in the thermal emission of carbon nanotubes. This is further corroborated by the partial polarization of the thermal emission spectra of metallic carbon nanotubes. We demonstrate that the temperature of semiconducting CNTs can be determined reliably by fitting these spectra to a Planck model in the visible wavelength range. The temperatures obtained from the G band Raman downshifts and Stokes/anti-Stokes Raman

intensity ratios agree well with the temperatures extracted from the IR spectra of semiconducting carbon nanotubes, despite non-equilibrium of the G_+ and G_- band phonon populations.

METHODS

Our sample fabrication proceeds as follows. A trench is first etched in a degenerately doped Si substrate capped with 1 μm of SiO_2 and 100 nm of silicon nitride. The nitride is dry-etched, and the underlying oxide is wet-etched to a depth of 500 nm. Pt contacts are then patterned perpendicular to the trench. Islands of Fe–Mo catalyst in an alumina matrix are then defined on top of the contacts in lithographically defined areas.[36] Nanotube growth is carried out by flowing a mixture of methane and hydrogen for 10 min at 825 °C. Devices that show negative differential conductance at high bias (1–2 V) with a maximum current of $\sim 10/L$ μA (where L is in μm) correspond to individual suspended single-walled nanotubes and are selected for further study.[3,37] Figure 1 shows one such device fabricated in this study. The optical image shows the thermal emission of the suspended portion of the CNT under a bias voltage of 2 V. Raman spectra and thermal emission spectra were measured in a Renishaw InVia spectrometer with 532 and 633 nm lasers. An Ithaco current preamplifier was used to measure the current passing through the nanotube. Our device is measured in an Ar environment at a pressure of 1 atm. For temperature calibration of IR spectra, we use a W lamp covered by a 5 μm pinhole. The temperature-induced downshifts in the nanotube Raman spectra are calibrated in a Linkam THMSE 600 temperature-controlled stage.

Acknowledgment. This research was supported in part by ONR Award No. N000141010511 (Z.L.), DOE Award No. DE-FG02-07ER46376 (M.A.), and NSF Award No. CBET-0854118 (A.B.). A portion of this work was done in the UCSB nanofabrication facility, part of the NSF funded NNIN network.

Supporting Information Available: Additional experimental details. This material is available free of charge *via* the Internet at http://pubs.acs.org.

REFERENCES AND NOTES

1. Cobden, D. H.; Bockrath, M.; McEuen, P. L.; Rinzler, A. G.; Smalley, R. E. Spin Splitting and Even-Odd Effects in Carbon Nanotubes. *Phys. Rev. Lett.* **1998**, *81*, 681–684.
2. Javey, A.; Guo, J.; Paulsson, M.; Wang, Q.; Mann, D.; Lundstrom, M.; Dai, H. J. High-Field Quasiballistic Transport in Short Carbon Nanotubes. *Phys. Rev. Lett.* **2004**, *92*, 106804.
3. Pop, E.; Mann, D.; Cao, J.; Wang, Q.; Goodson, K.; Dai, H. Negative Differential Conductance and Hot Phonons in Suspended Nanotube Molecular Wires. *Phys. Rev. Lett.* **2005**, *95*, 155505.
4. Deshpande, V. V.; Chandra, B.; Caldwell, R.; Novikov, D. S.; Hone, J.; Bockrath, M. Mott Insulating State in Ultraclean Carbon Nanotubes. *Science* **2009**, *323*, 106–110.
5. Bockrath, M.; Cobden, D. H.; Lu, J.; Rinzler, A. G.; Smalley, R. E.; Balents, L.; McEuen, P. L. Luttinger-Liquid Behaviour in Carbon Nanotubes. *Nature* **1999**, *397*, 598–601.
6. Radosavljevic, M.; Lefebvre, J.; Johnson, A. T. High-Field Electrical Transport and Breakdown in Bundles of Single-Wall Carbon Nanotubes. *Phys. Rev. B* **2001**, *64*, 241307.
7. Yao, Z.; Kane, C. L.; Dekker, C. High-Field Electrical Transport in Single-Wall Carbon Nanotubes. *Phys. Rev. Lett.* **2000**, *84*, 2941–2944.
8. Lazzeri, M; P., S.; Mauri, F; Ferrari, A. C.; Robertson, J Electron Transport and Hot Phonons in Carbon Nanotubes. *Phys. Rev. Lett.* **2005**, *95*, 236802.
9. Piscanec, S.; Lazzeri, M.; Robertson, J.; Ferrari, A. C.; Mauri, F. Optical Phonons in Carbon Nanotubes: Kohn Anomalies, Peierls Distortions, and Dynamic Effects. *Phys. Rev. B* **2007**, *75*, 035427.
10. Bushmaker, A. W.; Deshpande, V. V.; Bockrath, M. W.; Cronin, S. B. Direct Observation of Mode Selective Electron–Phonon Coupling in Suspended Carbon Nanotubes. *Nano Lett.* **2007**, *7*, 3618.
11. Bushmaker, A. W.; Deshpande, V. V.; Hsieh, S.; Bockrath, M. W.; Cronin, S. B. Gate Voltage Controlled Non-Equilibrium and Non-Ohmic Behavior in Suspended Carbon Nanotubes. *Nano Lett.* **2009**, *9*, 2862.
12. Deshpande, V. V.; Hsieh, S.; Bushmaker, A. W.; Bockrath, M.; Cronin, S. B. Spatially Resolved Temperature Measurements of Electrically Heated Carbon Nanotubes. *Phys. Rev. Lett.* **2009**, *102*, 105501.
13. Oron-Carl, M.; Krupke, R. Raman Spectroscopic Evidence for Hot-Phonon Generation in Electrically Biased Carbon Nanotubes. *Phys. Rev. Lett.* **2008**, *100*, 127401.
14. Steiner, M.; Freitag, M.; Perebeinos, V.; Tsang, J.; Small, J.; Kinoshita, M.; Yuan, D.; Liu, J.; Avouris, P. *Phonon Populations in a Biased Carbon Nanotube Transistor*, Bulletin of the American Physical Society, Pittsburgh, Pennsylvania, 2009.
15. Freitag, M.; Chiu, H. Y.; Steiner, M.; Perebeinos, V.; Avouris, P. Thermal Infrared Emission from Biased Graphene. *Nat. Nanotechnol.* **2010**, *5*, 497–501.
16. Berciaud, S.; Han, M. Y.; Mak, K. F.; Brus, L. E.; Kim, P.; Heinz, T. F. Electron and Optical Phonon Temperatures in Electrically Biased Graphene. *Phys. Rev. Lett.* **2010**, *104*, 227401.
17. Aliev, A. E.; Kuznetsov, A. A. The Origin of Polarized Blackbody Radiation from Resistively Heated Multiwalled Carbon Nanotubes. *Phys. Lett. A* **2008**, *372*, 4938–4942.
18. Li, P.; Jiang, K.; Liu, M.; Li, Q.; Fan, S. Polarized Incandescent Light Emission from Carbon Nanotubes. *Appl. Phys. Lett.* **2003**, *82*, 1763–1765.
19. Essig, S.; Marquardt, C. W.; Vijayaraghavan, A.; Ganzhorn, M.; Dehm, S.; Hennrich, F.; Ou, F.; Green, A. A.; Sciascia, C.; Bonaccorso, F.; *et al.* Phonon-Assisted Electroluminescence from Metallic Carbon Nanotubes and Graphene. *Nano Lett.* **2010**, *10*, 1589–1594.
20. Xie, L. M.; Farhat, H.; Son, H. B.; Zhang, J.; Dresselhaus, M. S.; Kong, J.; Liu, Z. F. Electroluminescence from Suspended and On-Substrate Metallic Single-Walled Carbon Nanotubes. *Nano Lett.* **2009**, *9*, 1747–1751.
21. Mann, D.; Kato, Y. K.; Kinkhabwala, A.; Pop, E.; Cao, J.; Wang, X.; Zhang, L.; Wang, Q.; Guo, J.; Dai, H. Electrically Driven Thermal Light Emission from Individual Single-Walled Carbon Nanotubes. *Nat. Nanotechnol.* **2007**, *2*, 33–38.
22. Freitag, M.; Steiner, M.; Naumov, A.; Small, J. P.; Bol, A. A.; Perebeinos, V.; Avouris, P. Carbon Nanotube Photo- and Electroluminescence in Longitudinal Electric Fields. *ACS Nano* **2009**, *3*, 3744–3748.
23. Fan, Y. W.; Singer, S. B.; Bergstrom, R.; Regan, B. C. Probing Planck's Law with Incandescent Light Emission from a Single Carbon Nanotube. *Phys. Rev. Lett.* **2009**, *102*, 4.
24. Wang, X.; Zhang, L.; Lu, Y.; Dai, H.; Kato, Y. K.; Pop, E. Electrically Driven Light Emission from Hot Single-Walled Carbon Nanotubes at Various Temperatures and Ambient Pressures. *Appl. Phys. Lett.* **2007**, *91*, 261102.
25. Freitag, M.; Steiner, M.; Martin, Y.; Perebeinos, V.; Chen, Z. H.; Tsang, J. C.; Avouris, P. Energy Dissipation in Graphene Field-Effect Transistors. *Nano Lett.* **2009**, *9*, 1883–1888.
26. Park, J. Y.; Rosenblatt, S.; Yaish, Y.; Sazonova, V.; Ustunel, H.; Braig, S.; Arias, T. A.; Brouwer, P. W.; McEuen, P. L. Electron–Phonon Scattering in Metallic Single-Walled Carbon Nanotubes. *Nano Lett.* **2004**, *4*, 517–520.
27. Araujo, P. T.; Jorio, A.; Dresselhaus, M. S.; Sato, K.; Saito, R. Diameter Dependence of the Dielectric Constant for the

Excitonic Transition Energy of Single-Wall Carbon Nanotubes. *Phys. Rev. Lett.* **2009**, *103*, 146802.
28. Strano, M. S.; Dyke, C. A.; Usrey, M. L.; Barone, P. W.; Allen, M. J.; Shan, H.; Kittrell, C.; Hauge, R. H.; Tour, J. M.; Smalley, R. E. Electronic Structure Control of Single-Walled Carbon Nanotube Functionalization. *Science* **2003**, *301*, 1519–1522.
29. Malyutenko, V. K. Thermal Emission of Semiconductors: Inverstigation and Application. *Infrared Phys.* **1991**, *32*, 291–302.
30. Jones, H. A. A Temperature Scale for Tungsten. *Phys. Rev.* **1926**, *28*, 202–207.
31. Hsu, I.-K.; Kumar, R.; Bushmaker, A.; Cronin, S. B.; Pettes, M. T.; Shi, L.; Brintlinger, T.; Fuhrer, M. S.; Cumings, J. Optical Measurement of Thermal Transport in Suspended Carbon Nanotubes. *Appl. Phys. Lett.* **2008**, *92*, 063119.
32. Cronin, S. B.; Yin, Y.; Walsh, A.; Capaz, R. B.; Stolyarov, A.; Tangney, P.; Cohen, M. L.; Louie, S. G.; Swan, A. K.; Unlü, M. S.; *et al*. Temperature Dependence of the Optical Transition Energies of Carbon Nanotubes: The Role of Electron−Phonon Coupling and Thermal Expansion. *Phys. Rev. Lett.* **2006**, *96*, 127403.
33. Spataru, C. D.; Ismail-Beigi, S.; Benedict, L. X.; Louie, S. G. Excitonic Effects and Optical Spectra of Single-Walled Carbon Nanotubes. *Phys. Rev. Lett.* **2004**, *92*, 077402.
34. Kane, C. L.; Mele, E. J. Electron Interactions and Scaling Relations for Optical Excitations in Carbon Nanotubes. *Phys. Rev. Lett.* **2004**, *93*, 197402.
35. Walsh, A. G.; Vamivakas, A. N.; Yin, Y.; Cronin, S. B.; Unlu, M. S.; Goldberg, B. B.; Swan, A. K. Scaling of Exciton Binding Energy with External Dielectric Function in Carbon Nanotubes. *Physica E* **2008**, *40*, 2375–2379.
36. Cao, J.; Wang, Q.; Wang, D.; Dai, H. Suspended Carbon Nanotube Quantum Wires with Two Gates. *Nanotube Devices* **2005**, *1*, 138–141.
37. Kong, J.; Soh, H. T.; Cassell, A. M.; Quate, C. F.; Dai, H. Synthesis of Individual Single-Walled Carbon Nanotubes on Patterned Silicon Wafers. *Nature* **1998**, *395*, 878–881.